Field-Induced Rocking-Curve Effects in Attosecond Electron Diffraction

Y. Morimoto [1,2,3,*] and P. Baum [1,†]

[1]Universität Konstanz, Fachbereich Physik, 78464 Konstanz, Germany
[2]RIKEN Cluster for Pioneering Research and RIKEN Center for Advanced Photonics, RIKEN 351-0198, Wako, Saitama, Japan
[3]Department of Nuclear Engineering and Management, Graduate School of Engineering, The University of Tokyo, 7-3-1 Hongo, Bunkyo-ku, Tokyo 113-8656, Japan

(Received 6 November 2023; accepted 15 April 2024; published 22 May 2024)

Recent advances in electron microscopy trigger the question of whether attosecond electron diffraction can resolve atomic-scale electron dynamics in crystalline materials in space and time. Here, we explore the ultrafast dynamics of the relevant electron-lattice scattering process. We drive a single-crystalline silicon membrane with the optical cycles of near-infrared laser light and use phase-locked attosecond electron pulses to produce electron diffraction patterns as a function of delay. For all Bragg spots, we observe time-dependent intensity changes and position shifts that are correlated with a time shift of 0.5–1.2 fs. For single-cycle excitation pulses with strong peak intensity, the correlations become nonlinear. The origins of these effects are local and integrated beam deflections by the optical electric and magnetic fields at the crystal membrane. Those deflections modify the diffraction intensities in addition to the atomic structure factor dynamics by time-dependent rocking-curve effects. However, the measured time delays and symmetries allow one to disentangle both effects. Future attosecond electron diffraction and microscopy experiments need to be based on these results.

DOI: 10.1103/PhysRevLett.132.216902

Ultrafast pump-probe experiments with pulsed electron beams [1–3] or x-ray sources [4,5] can resolve the motion of atoms in space and time. However, the primary response of a material to light is given by the motion of electrons in the electromagnetic excitation wave in times as short as attoseconds. In order to see such dynamics, ultrafast electron microscopy has recently been advanced from the femtosecond into the attosecond domain [6,7], based on pioneering concepts for laser-electron control [6–18]. Advanced interferometric electron microscopy even allows one to detect optical near-field phases without attosecond pulses [19,20]. However, the spatial resolution is not at atomic dimensions yet, and additional efforts are therefore appropriate.

A potential solution for merging subatomic resolution in space with attosecond information in time is attosecond electron diffraction. Figure 1(a) shows the basics of such an experiment. A crystalline material (green) is excited by the electric field cycles of laser light (red), pushing and pulling electron densities between the atoms [21] and along the chemical bonds [22]. During this motion, synchronized attosecond electron pulses [6,10–15] (blue) produce an electron diffraction pattern as a function of time delay. In theory [21], the diffraction intensities then reveal the microscopic electronic motion on atomic scales [21,23–25].

However, all simulations and preliminary experiments [6] so far ignore the unavoidable presence of the optical excitation fields. While the Kroll-Watson formula [26] guarantees for isolated atoms a safe extraction of the form factor from energy-integrated diffraction intensities, there is no such theorem on the diffraction by crystals with their periodic atom lattice. It, therefore, remains to be resolved how electron diffraction from condensed matter works on attosecond timescales and how time-dependent Bragg spot intensity changes relate to the attosecond dynamics of the investigated material and its internal optical fields.

In our experiments, we excite a single-crystalline membrane of silicon (green) with a thickness of $d = 60$ nm with the optical cycles of femtosecond laser light at $\lambda = 1030$ nm wavelength (red). Attosecond electron pulses [6] at an energy of 70 keV and velocity of $v_e = 0.48c$ (blue) diffract from the crystal lattice into Bragg spots on a detector screen (gray). The attosecond electron pulses that are locked to the excitation field cycles hit the silicon membrane at ∼35° under a surface normal in $[-1/\sqrt{2}, \sqrt{2}, 1/\sqrt{2}]$ direction and produce Bragg diffraction.

Figure 1(b) shows the diffraction pattern that we obtain with our train of attosecond electron pulses without laser excitation [6]. We see Bragg spots at a large variety of Miller indices. When we apply the pump laser field (p polarization, 145° incidence, pulse duration 1.7 ps, electric peak field strength $F = 0.2$ V/nm), we observe a periodic deflection of the Bragg spots on attosecond timescales; see Figs. 1(c) and 1(d). Also, the Bragg spot intensities are modulated as a function of time; see Fig. 1(e). We integrate over ∼4 times the spot size plus deflection amplitude. The measured

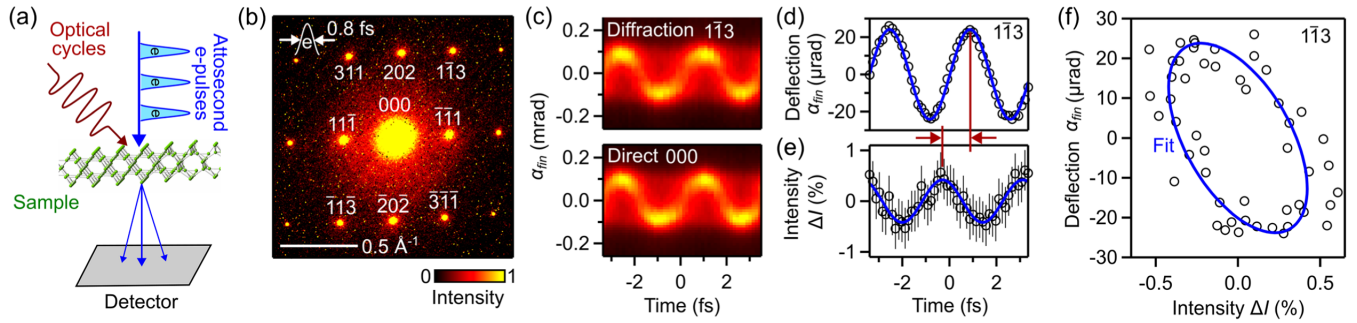

FIG. 1. Attosecond electron diffraction and measured time delays. (a) Concept and experiment. A crystalline material (green) is excited by the optical cycles of laser light (red) and then investigated with attosecond electron pulse trains (blue). (b) Attosecond diffraction pattern of a Si crystal without laser excitation. The electron pulse length is 0.8 fs (white). (c) Raw data of the observed Bragg spot dynamics as a function of delay time. (d) Time-resolved center-of-mass motion of the $1\bar{1}3$ Bragg spot. (e) Time-resolved total diffraction intensity. The red lines and arrows indicate a time delay. (f) Correlation between sideways streaking (vertical axis) and diffraction intensity (horizontal axis). Blue line is a double-sinusoidal fit.

intensity changes are almost 1%, determined by the contrast and background in the attosecond train [6].

The intensity oscillations $\Delta I(t)$ have the same period as the deflections $\alpha_{\mathrm{fin}}(t)$ but appear with a substantial time delay (red marks). Figure 1(f) shows a correlation plot, accumulated over all attosecond time delays. We see an elliptical pattern with a tilt (blue). A positively deflected $1\bar{1}3$ Bragg spot has generally less intensity than a negatively deflected $1\bar{1}3$ spot but the correlation is not direct: unchanged intensities, for example, occur at two distinct deflections and time delays. A least-square fitting (blue) with two phase-shifted sinusoidal oscillation curves reveals a time delay of -1.17 ± 0.08 fs or a phase delay of -2.14 ± 0.07 rad between beam deflection $\alpha_{\mathrm{fin}}(t)$ and intensity modulation $\Delta I(t)$. These values are substantial and far away from any multiple of π or $\pi/2$; in other words, the measured ellipse is neither a line nor a circle. The seven other Bragg spots show very similar effects (see below).

In order to understand the measured attosecond beam deflections, we look at the electron trajectories close to the specimen; see Fig. 2(a). While the attosecond electron pulses (blue) pass through the optical focus (red) and the silicon crystal (green), they accumulate from the time-integrated electromagnetic fields a final sideways deflection (blue) because the material breaks the symmetry of a free-space interaction and enables electron-photon momentum exchange [8,27–30]. Consequently, the direct electron beam and all far-field Bragg diffractions rapidly oscillate on the screen as a function of electron arrival time.

In order to understand the measured attosecond intensity changes, we first estimate what effects can be expected from atomic-scale electron dynamics [21]. Density-functional theory with a static-field approximation [6] reveals that the expected intensity changes for our material and laser intensity are merely 0.01% and should appear at twice the frequency of the excitation field [21], because left-driven atomic charges and right-driven atomic charges produce the same Bragg spot changes due to Friedel's law. However, the measured Bragg spot changes appear at the fundamental laser frequency. Our observed intensity oscillations can therefore not be explained by changes of the scattering form factor and field-driven electronic motions on atomic dimensions.

Instead, the scattering process itself is modified by the presence of the excitation light. The optical laser fields (red) not only excite the specimen but also induce an unavoidable quiver motion of the incoming attosecond electron pulses (blue), and the electrons pass through the specimen at special instantaneous angles that are determined by the interaction geometry. In our experiment, the train of attosecond electron pulses receives oscillating electric and magnetic forces in the $x-z$ plane and enters the crystal at an angle $\alpha_{\mathrm{sample}}(t)$, which is determined by the integrated laser fields of the left half of the geometry. The continuing oscillations in the remaining laser fields only contribute to the final far-field deflection [8,27,30,31].

Electron diffraction at a nonoptimized angle of incidence causes Bragg spot attenuation due to rocking-curve effects. Figure 2(b) depicts the reciprocal crystal lattice (black) together with the Ewald sphere (blue). Provided that the time it takes to diffract into Bragg spots ($d/v_e \approx 0.4$ fs) is shorter than half an optical cycle period (1.7 fs), the local angle $\alpha_{\mathrm{sample}}(t)$ is approximately well-defined. An oscillating $\alpha_{\mathrm{sample}}(t)$ on attosecond dimensions (dotted blue lines) therefore creates a rapidly quivering Ewald sphere (dashed blue circles) that rotates periodically around the origin O at the frequency of the laser light. This ultrafast rotation increases or decreases the overlap with the reciprocal lattice points and modulates the measured diffraction intensities. Importantly, the oscillation period is the same as the laser period and opposite Bragg spots (Friedel pairs) obtain approximately opposite effects.

Figure 2(c) depicts several measured rocking curves in our experiment, that is, electron diffraction intensities under

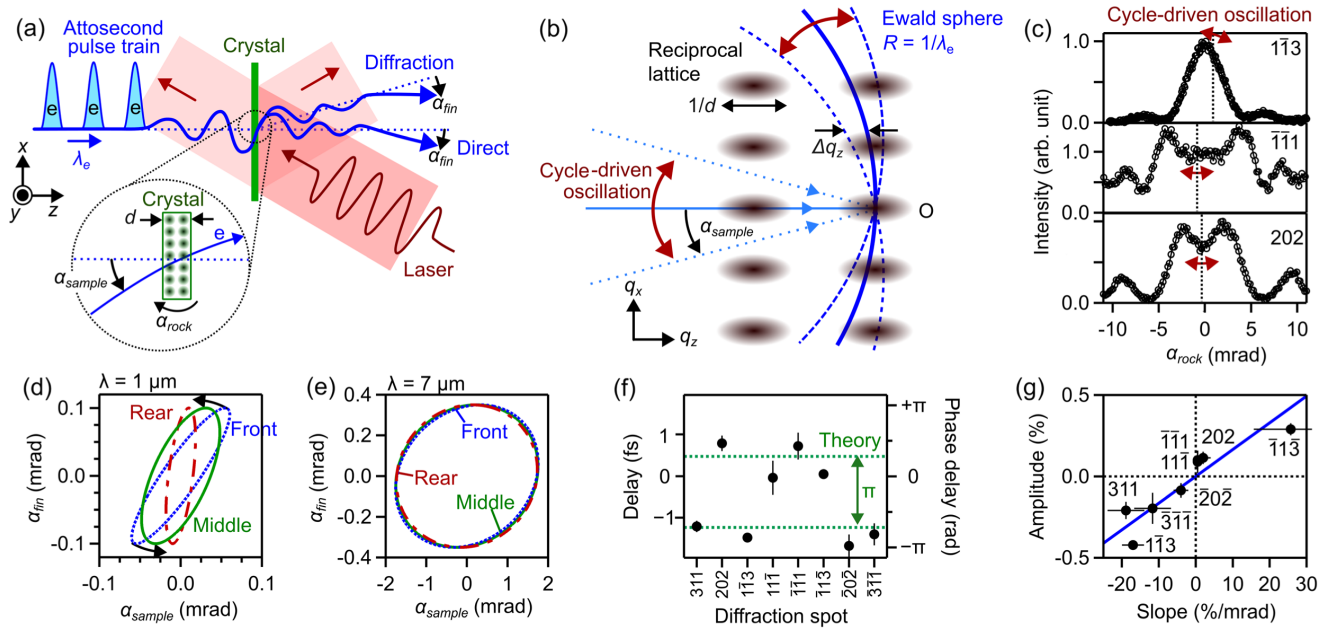

FIG. 2. Attosecond rocking-curve effect. (a) Details of the experiment. α_{sample}, instantaneous beam deflection; α_{fin}, final beam deflection; α_{rock}, static material angle; λ_e, electron de Broglie wavelength; d, crystal thickness. (b) Reciprocal-space dynamics. The cycle-driven rotation of the Ewald sphere (blue) modulates the overlap with the reciprocal lattice (black). R, radius of the Ewald sphere; O, origin; Δq_z, shift of the Ewald sphere along q_z. (c) Measured rocking curves for three diffraction spots. (d) Simulated phase delay of $\alpha_{\mathrm{sample}}(t)$ with respect to $\alpha_{\mathrm{fin}}(t)$ for 1-μm laser light. (e) Simulated phase delay of $\alpha_{\mathrm{sample}}(t)$ with respect to $\alpha_{\mathrm{fin}}(t)$ for 7-μm laser light. (f) Measured time delays for eight different Bragg diffraction spots. (g) Measured intensity modulation amplitudes in correlation to measured rocking-curve derivatives. Blue line, linear fit.

systematic variation of the angle of incidence α_{rock}. Attosecond electron pulses or a continuous beam yield almost identical results. We see for the $1\bar{1}3$ spot an almost Gaussian curve while the $\bar{1}\bar{1}1$ and 202 spots have dips in the middle due to multiple scattering effects [32]. The black dotted lines are the static angles of the attosecond experiment, and the red arrows indicate the oscillation of $\alpha_{\mathrm{sample}}(t)$ due to the optical cycles of the pump laser field. The slope and curvature of the rocking curve at the chosen diffraction geometry therefore translates the attosecond quivering of the electron beam into attosecond modulations of measured Bragg spot intensities. Afterward, the entire diffraction pattern continues to transverse the remaining laser fields until an angularly oscillating far-field pattern is produced.

To confirm these explanations, we relate $\alpha_{\mathrm{sample}}(t)$ and $\alpha_{\mathrm{fin}}(t)$ by theory. The electrons and laser fields are treated as point particles and plane waves, respectively [8,31], and optical thin-film interferences are taken into full account; see Ref. [8] and Supplemental Material [33]. Quantum effects are not relevant to our experiments because the lateral coherence of the electron beam of ~20 nm [37] is much smaller than the optical wavelength and thus not enough to observe quantized deflection [27,30]. The coherence is, however, much larger than a unit cell, leading to the observation of Bragg spots. Figure 2(d) shows the simulated $\alpha_{\mathrm{sample}}(t)$ and $\alpha_{\mathrm{fin}}(t)$ at three essential points of the specimen (front surface, middle, and rear surface). All ellipses show substantial areas and, therefore, time delays. They are not all equal because the time of electron diffraction ($d/v_e = 0.4$ fs) is not entirely irrelevant with respect to the optical cycle period (3.4 fs). In the experiment, we measure an average of all three dynamics and, therefore, consider here the middle one (green) for further analysis. The theoretical delay between $\alpha_{\mathrm{sample}}(t)$ and $\alpha_{\mathrm{fin}}(t)$ is 0.48 fs or 0.88 rad but the rocking-curve slope is negative, that is, a positive α_{sample} decreases the diffraction intensity. The delay between $\Delta I(t)$ and $\alpha_{\mathrm{fin}}(t)$ is therefore $0.88\ \mathrm{rad} - \pi = -2.3$ rad, which matches well with the experiment (−2.1 rad).

To obtain a more systematic picture, we repeat our experiments for the other seven diffraction spots. For each Bragg spot, we align the crystal slightly away from the optimum Bragg condition by 0.07 ± 0.05 mrad, which is the accuracy of our goniometer mechanics. Figure 2(f) shows the extracted time delays between $\Delta I(t)$ and $\alpha_{\mathrm{fin}}(t)$. Values around −1.2 fs correspond to the theoretical prediction (lower green line), indicating a negative slope of the rocking curve (for example, $1\bar{1}3$), while values around +0.5 fs (upper green line) correspond to Bragg spots with positive rocking-curve derivative (for example, 202). Figure 2(g) shows the measured intensity oscillation amplitudes for each Bragg spot as a function of the slope of the corresponding rocking curve, postcharacterized after each attosecond measurement. As expected, the results are approximately on a straight line (blue).

Before reporting more experiments, we make some intermediate conclusions: First, the observed attosecond modulations of Bragg spot intensities are not specific for our experimental geometry but general for any experiments in which a laser excitation (or its reflection) drives atomic-scale dynamics in a perpendicular direction to the electron beam [21]. Any such sideways fields produce attosecond rocking-curve effects [33]. Second, the modulation amplitude of $\alpha_{\mathrm{sample}}(t)$ scales proportionally to F, λ, and $1/v_e$ [8,38], that is, the modulation becomes stronger with higher field amplitude, weaker for shorter excitation wavelengths, and stronger for slower electrons. Thicker crystals will have stronger modulation effects due to their sharper rocking curves. Third, the reported rocking-curve effects are stronger for higher-order Bragg diffractions because the shift of the Ewald sphere, $\Delta q_z(q_x,t) \approx \alpha_{\mathrm{sample}}(t) q_x$ in Fig. 2(b), is larger there. In contrast, modulations from electronic motion on atomic dimensions are stronger at lower Miller indices due to the dominant contribution of outer electrons far from the cores [21]. The attosecond rocking-curve effect originates predominantly from the periodicity of the lattice and is independent of potential electron dynamics and the associated structure factors, provided that the unit-cell size and its symmetry are maintained; see Supplemental Material [33]. Therefore, a combined measurement of multiple Bragg diffraction orders or measurements of time-dependent rocking curves can discern these two effects.

Next, we use single-cycle excitation pulses and explore the onset of nonlinearities in attosecond electron diffraction in strong laser fields. Figure 3(a) depicts the new experimental geometry. The excitation pulses (red) are now obtained from a midinfrared optical parametric amplifier [39] that provides ~20 times shorter pulses (36 fs) and ~7 times longer optical cycles (wavelength 6.9 μm) than before. The carrier-envelope phase is not locked, and the electron pulses have a duration of ~800 fs [40]. Bragg spot data is therefore averaged over all time delays [41]. Nevertheless, each measured beam deflection still can be assigned to a measured diffraction intensity for extracting correlations and delays. Figure 3(b) shows the measured far-field streaking of the $\bar{1}1\bar{3}$ Bragg spot (upper panel) in comparison to the dynamics of the direct beam (lower panel). With the pump laser on ($F = 0.5$ V/nm), both electron beams obtain a substantial broadening in x direction (right panels). We focus our analysis on signals with $|\alpha_{\mathrm{fin}}| > 0.2$ mrad, where electrons must have interacted with strong parts of the excitation field [41].

Figure 3(c) shows the measured rocking curve and the two dotted lines indicate two intentional misalignments. For a rather low misalignment of 0.9 mrad, the left panel of Fig. 3(d) shows the simulated correlation diagram (green line). The laser field is now so strong that the oscillations of $\alpha_{\mathrm{sample}}(t)$ are comparable to the width of the rocking curve and drive for some delays the instantaneous electron

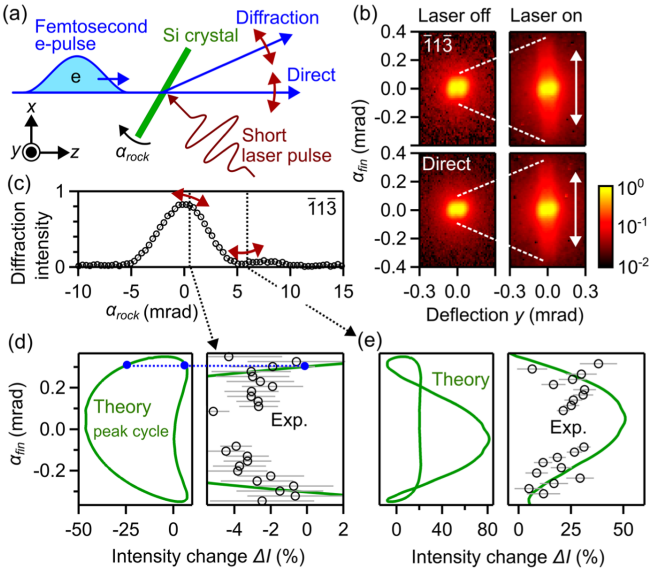

FIG. 3. Nonlinear modulation of electron-lattice scattering. (a) Schematic of the experiment. (b) Measured time-integrated sideways streaking (white arrows) of the $1\bar{1}3$ spot (upper panels) and the direct beam (lower panels). (c) Rocking curve. The black dotted lines denote two conditions of the experiment with their corresponding attosecond dynamics (red arrows). (d) Left panel: simulated correlation of diffraction intensity and final streaking angle (green) at $\alpha_{\mathrm{rock}} = 0.9$ mrad. Right panel: comparison with the experimental results (black circles). Two theoretical final deflections (blue dots) are indistinguishable in our experiment (no time resolution) and green curve therefore shows the theoretical average. Also, comparison is restricted to $|\alpha_{\mathrm{fin}}| > 0.2$ mrad in order to exclude the potential contributions of secondary laser cycles (~60% field strength). (e) Left: simulated correlation of diffraction intensity and final streaking angle (green) at $\alpha_{\mathrm{rock}} = 6$ mrad. Right: comparison angle-averaged theory (green) with the experimental results (black circles). Contributions from weaker optical cycle ($\leq 60\%$ field strength) that appear at small $|\alpha_{\mathrm{fin}}|$ are again neglected.

diffraction over the top into regions with negative derivative. Consequently, the correlation ellipse becomes distorted and one side even bends inside. The right panel of Fig. 3(d) shows the measured changes in total diffraction intensities ΔI at each deflection angle α_{fin}. Values are normalized to the measured total intensities of the direct plus diffracted beams that are observed at the same angle α_{fin}. Each measured Bragg spot and its corresponding reference are therefore filtered in the same way into a short temporal window of subcycle duration, and the results become independent of excess electrons that are far away in time [41]. As shown by the blue dotted line, there are two timings per laser cycle (blue dots) that result in the same α_{fin} and the average of these two instantaneous intensities gives the diffraction intensity of the experiment. We see a reasonable agreement, demonstrating that attosecond rocking curve effects are substantial in strongly field-driven

electron diffraction experiments even if no particularly short electron pulses are applied.

Figure 3(e) shows the results when we align the $\bar{1}1\bar{3}$ Bragg spot into a local minimum of the rocking curve at ~6 mrad. The left panel again shows the simulation results (green curve), revealing approximately a Lissajous figure with the laser frequency in $\alpha_{\mathrm{fin}}(t)$ direction and the sum of its second and third harmonics in $\Delta I(t)$ direction. The origin of these dynamics is the quadratic (symmetric) and cubic (antisymmetric) response of the rocking curve around its minimum. The right panel shows the measured intensity data (black circles) as a function of α_{fin}. The match demonstrates that the nonlinearity of the rocking curve is translated into nonlinear intensity dynamics in strongly field-driven electron diffraction.

The combined results show that the scattering process in ultrafast electron diffraction from crystalline materials is affected by the instantaneous electric and magnetic fields of the optical cycles of the excitation light. Whenever there are sideways electric fields in a material that can induce electronic motion into a crystallographic direction that would be observable by structure factor dynamics [21], there will also be time-dependent instantaneous beam deflections and rocking-curve effects. Although the final beam deflection effect can indeed become zero at special angle combinations [8,31], the rocking-curve effects remain at work [33]. Experiments with single-cycle excitation and isolated attosecond electron pulses [15,42] will be subject to the same effects. Fortunately, the results presented here allow one to disentangle the attosecond dynamics of the electron-lattice scattering process from atomic structure-factor effects by recording multiple Bragg spots or entire rocking curves as a function of delay. Attosecond electron diffraction, therefore, remains a feasible and useful next step for advancing attosecond electron imaging to the atomic resolution regime.

The data supporting the findings of this study are available from the corresponding author upon reasonable request.

We thank Bo-Han Chen for helpful discussions on optics. This research was supported by the German Research Foundation (DFG) via SFB 1432, the Vector Foundation, the Dr. K. H. Eberle Foundation, JST ACT-X JPMJAX21AO, JST FOREST, MEXT/JSPS KAKENHI JP21K21344, the Kazato Research Foundation, and the Research Foundation for Opto-Science and Technology.

*Corresponding author: yuya.morimoto@riken.jp
†Corresponding author: peter.baum@uni-konstanz.de

[1] A. H. Zewail, Four-dimensional electron microscopy, Science **328**, 187 (2010).
[2] R. J. D. Miller, Femtosecond crystallography with ultrabright electrons and x-rays: Capturing chemistry in action, Science **343**, 1108 (2014).
[3] D. Filippetto, P. Musumeci, R. K. Li, B. J. Siwick, M. R. Otto, M. Centurion, and J. P. F. Nunes, Ultrafast electron diffraction: Visualizing dynamic states of matter, Rev. Mod. Phys. **94**, 045004 (2022).
[4] B. W. J. McNeil and N. R. Thompson, X-ray free-electron lasers, Nat. Photonics **4**, 814 (2010).
[5] H. N. Chapman *et al.*, Femtosecond x-ray protein nanocrystallography, Nature (London) **470**, 73 (2011).
[6] Y. Morimoto and P. Baum, Diffraction and microscopy with attosecond electron pulse trains, Nat. Phys. **14**, 252 (2018).
[7] D. Nabben, J. Kuttruff, L. Stolz, A. Ryabov, and P. Baum, Attosecond electron microscopy of sub-cycle optical dynamics, Nature (London) **619**, 63 (2023).
[8] Y. Morimoto and P. Baum, Attosecond control of electron beams at dielectric and absorbing membranes, Phys. Rev. A **97**, 033815 (2018).
[9] Y. Morimoto, Attosecond electron-beam technology: A review of recent progress, Microscopy **72**, 2 (2023).
[10] K. E. Priebe, C. Rathje, S. V. Yalunin, T. Hohage, A. Feist, S. Schäfer, and C. Ropers, Attosecond electron pulse trains and quantum state reconstruction in ultrafast transmission electron microscopy, Nat. Photonics **11**, 793 (2017).
[11] M. Kozák, N. Schönenberger, and P. Hommelhoff, Ponderomotive generation and detection of attosecond free-electron pulse trains, Phys. Rev. Lett. **120**, 103203 (2018).
[12] N. Schönenberger, A. Mittelbach, P. Yousefi, J. McNeur, U. Niedermayer, and P. Hommelhoff, Generation and characterization of attosecond microbunched electron pulse trains via dielectric laser acceleration, Phys. Rev. Lett. **123**, 264803 (2019).
[13] D. S. Black, U. Niedermayer, Y. Miao, Z. Zhao, O. Solgaard, R. L. Byer, and K. J. Leedle, Net acceleration and direct measurement of attosecond electron pulses in a silicon dielectric laser accelerator, Phys. Rev. Lett. **123**, 264802 (2019).
[14] A. Ryabov, J. W. Thurner, D. Nabben, M. V. Tsarev, and P. Baum, Attosecond metrology in a continuous-beam transmission electron microscope, Sci. Adv. **6**, abb1393 (2020).
[15] Y. Morimoto and P. Baum, Single-cycle optical control of beam electrons, Phys. Rev. Lett. **125**, 193202 (2020).
[16] R. Dahan *et al.*, Resonant phase-matching between a light wave and a free-electron wavefunction, Nat. Phys. **16**, 1123 (2020).
[17] B. Barwick, D. J. Flannigan, and A. H. Zewail, Photon-induced near-field electron microscopy, Nature (London) **462**, 902 (2009).
[18] A. Feist, K. E. Echternkamp, J. Schauss, S. V. Yalunin, S. Schäfer, and C. Ropers, Quantum coherent optical phase modulation in an ultrafast transmission electron microscope, Nature (London) **521**, 200 (2015).
[19] J. H. Gaida, H. Lourenço-Martins, M. Sivis, T. Rittmann, A. Feist, F. J. García de Abajo, and C. Ropers, Attosecond electron microscopy by free-electron homodyne detection, Nat. Photonics (2024).
[20] T. Bucher, R. Ruimy, S. Tsesses, R. Dahan, G. Bartal, G. M. Vanacore, and I. Kaminer, Free-electron Ramsey-type

interferometry for enhanced amplitude and phase imaging of nearfields, Sci. Adv. **9**, eadi572 (2023).
[21] V. S. Yakovlev, M. I. Stockman, F. Krausz, and P. Baum, Atomic-scale diffractive imaging of sub-cycle electron dynamics in condensed matter, Sci. Rep. **5**, 14581 (2015).
[22] Y. Morimoto, Y. Shinohara, M. Tani, B.-H. Chen, K. L. Ishikawa, and P. Baum, Asymmetric single-cycle control of valence electron motion in polar chemical bonds, Optica **8**, 382 (2021).
[23] H.-C. Shao and A. F. Starace, Detecting electron motion in atoms and molecules, Phys. Rev. Lett. **105**, 263201 (2010).
[24] G. Dixit, O. Vendrell, and R. Santra, Imaging electronic quantum motion with light, Proc. Natl. Acad. Sci. U.S.A. **109**, 11636 (2012).
[25] P. Baum, J. Manz, and A. Schild, Quantum model simulations of attosecond electron diffraction, Sci. China Phys. Mech. Astron. **53**, 987 (2010).
[26] N. M. Kroll and K. M. Watson, Charged-particle scattering in the presence of a strong electromagnetic wave, Phys. Rev. A **8**, 804 (1973).
[27] G. M. Vanacore *et al.*, Attosecond coherent control of free-electron wave functions using semi-infinite light fields, Nat. Commun. **9**, 2694 (2018).
[28] T. Plettner, R. L. Byer, E. Colby, B. Cowan, C. M. S. Sears, J. E. Spencer, and R. H. Siemann, Visible-laser acceleration of relativistic electrons in a semi-infinite vacuum, Phys. Rev. Lett. **95**, 134801 (2005).
[29] F. O. Kirchner, A. Gliserin, F. Krausz, and P. Baum, Laser streaking of free electrons at 25 KeV, Nat. Photonics **8**, 52 (2014).
[30] A. Feist, S. V. Yalunin, S. Schäfer, and C. Ropers, High-purity free-electron momentum states prepared by three-dimensional optical phase modulation, Phys. Rev. Res. **2**, 043227 (2020).
[31] D. Ehberger, A. Ryabov, and P. Baum, Tilted electron pulses, Phys. Rev. Lett. **121**, 094801 (2018).
[32] M. Ligges, I. Rajković, C. Streubühr, T. Brazda, P. Zhou, O. Posth, C. Hassel, G. Dumpich, and D. von der Linde, Transient (000)-order attenuation effects in ultrafast transmission electron diffraction, J. Appl. Phys. **109**, 063519 (2011).
[33] See Supplemental Material at http://link.aps.org/supplemental/10.1103/PhysRevLett.132.216902 for the detailed theoretical discussions, which includes Refs. [34–36].
[34] L. Landau and Evgeny Lifshitz, *The Classical Theory of Fields, Course of Theoretical Physics* (Elsevier Science, New York, 1975), Vol. 2.
[35] H.-C. Shao and A. F. Starace, Imaging coherent electronic motion in atoms by ultrafast electron diffraction, Phys. Rev. A **88**, 062711 (2013).
[36] C. Kittel, *Introduction to Solid State Physics*, 7th ed. (Wiley, New York, 1996).
[37] F. O. Kirchner, S. Lahme, F. Krausz, and P. Baum, Coherence of femtosecond single electrons exceeds biomolecular dimensions, New J. Phys. **15**, 063021 (2013).
[38] C. J. Joachain, N. J. Kylstra, and R. M. Potvliege, *Atoms in Intense Laser Fields* (Cambridge University Press, New York, 2011).
[39] B.-H. Chen, E. Wittmann, Y. Morimoto, P. Baum, and E. Riedle, Octave-spanning single-cycle middle-infrared generation through optical parametric amplification in $LiGaS_2$, Opt. Express **27**, 21306 (2019).
[40] C. Kealhofer, W. Schneider, D. Ehberger, A. Ryabov, F. Krausz, and P. Baum, All-optical control and metrology of electron pulses, Science **352**, 429 (2016).
[41] Y. Morimoto, B. Chen, and P. Baum, Free-electron tomography of few-cycle optical waveforms, Ann. Phys. (Amsterdam) **534**, 2200193 (2022).
[42] M. Kozák, All-optical scheme for generation of isolated attosecond electron pulses, Phys. Rev. Lett. **123**, 203202 (2019).